AN EMBEDDED IOT ANTENNA FOR SMART PAVEMENT MONITORING SYSTEM

BY

SHUO LIU

THESIS

Submitted in partial fulfillment of the requirements
for the degree of Master of Science in Electrical and Computer Engineering
in the Graduate College of the
University of Illinois at Urbana-Champaign, 2018

Urbana, Illinois

Adviser:

Professor Jennifer Bernhard

Abstract

To support the design of compact IoT devices, a general procedure for developing IoT antennas will be illustrated in this work. The design steps are based on the study of an embedded antenna used in a smart pavement monitoring system which has been introduced to monitor pavement conditions and make plans for road rehabilitation. In order to overcome the drawbacks of traditional patch antennas used in road pavement, a ground plane serration technique has been studied and applied to the proposed antenna to improve its performance. Simulation and measurement results show that with serrations on the ground plane, the proposed antenna is able provide broadside gain of 3.4 dB through asphalt pavement.

Acknowledgments

I would like to thank Professor Jennifer Bernhard for her continual support, guidance and encouragement to help me finish this research. I would also like to thank my group members for giving me valuable insights and helping me solve problems during the study. Finally, I would like to thank my parents for supporting me to finish my master's degree.

Contents

Chapter 1 Introduction 1

Chapter 2 Background 3

2.1 Smart Pavement Monitoring System 3

2.2 Previous Work 5

2.2.1 Standard Patch Antenna Used under Pavement 5

2.2.2 Standard Loop Antenna Used under Pavement 7

2.2.3 Low-profile Antennas for IoT Applications 9

2.2.4 Summary for Background 9

Chapter 3 Theory 11

3.1 Overview 11

3.2 Design Procedure 11

3.2.1 Antenna Selection 11

3.2.2 Frequency Selection 12

3.2.3 Model Construction 13

3.2.4 Ground Plane Issue 16

3.2.5 Ground Plane Improvement 18

3.2.6 Pavement Sensitivity Analysis 21

Chapter 4 Measurement 26

4.1 Antenna Fabrication 26

4.2 Pattern Measurement 28

4.3 Results 29

Chapter 5 Conclusion and Future Work 32

5.1 Conclusion 32

5.2 Future Work 33

References 34

Chapter 1

Introduction

Internet of Things (IoT) is one of the fastest developing technologies in recent years. It can be defined as a network that connects physical objects to collect and access real-life information. IoT technology enables easy connections between objects and therefore allows more efficient information delivery than traditional communication tools. In the near future, thousands of devices are expected to be connected to the Internet where they can smartly collect and share data necessary for making intelligent actions or decisions.

As technology continues to advance, the trend is toward an interconnected world that is supported by numerous portable and compact IoT devices. Meanwhile, to realize the miniaturization of electronic devices, antennas, which are the key component for wirelessly delivering information, need to be improved in terms of reducing size while maintaining the gain and bandwidth. In the last several years, engineers have kept researching and pushing new designs of antennas which can be applied to IoT applications in different areas. For instance, with the use of IoT technology, smart embedded devices have been playing an important role in remotely sensing and monitoring health and wellness information for infrastructures such as roads and bridges [1] – [3]. In order to realize an embedded IoT device, the antenna responsible for sending signals should be designed to enable packaging it in a box which is buried under the pavement.

Although there are plenty of research examples of specific embedded antennas for IoT applications, little effort has been made to generalize from these examples. In fact, embedded IoT antennas share some common design and development procedures that merit study.

In order to illustrate the general method to design such antennas, a special case of embedded IoT antenna for a smart pavement monitoring system is researched and developed. Background

together with previous work on smart pavement monitoring systems will be provided in Chapter 2. In Chapter 3, design procedures of general IoT antennas based on the antenna in the special case will be studied. Chapter 4 will provide measurement procedures and results for the antenna. Finally, Chapter 5 summarizes the completed work and discusses ideas for future work. The thesis can serve as a general reference for the design of embedded IoT antennas.

Chapter 2

Background

2.1 Smart Pavement Monitoring System

Roads are one of the most important components of a country's infrastructure. Their condition greatly affects the efficiency of transportation, on which a nation's economy relies. However, because most of the roads in the US were constructed a half century or more ago, many of them are deteriorating and in need of repair. To ensure the safety of road travel, for example, the state of Illinois has been spending billions of dollars on road reconstruction and maintenance every year [4]. To reduce the cost of road maintenance, the smart pavement monitoring system has been proposed. This system enables the prediction of road conditions and helps to plan road rehabilitation by providing real-time environment data in the pavement, such as pressure, temperature, humidity, and salinity.

There are two general approaches to construct the monitoring system. The first one, proposed in [5], is illustrated in Figure 1. As is shown, the system contains a network of low-cost sensors distributed under the pavement. Each sensor node is self-powered and can continuously monitor the pavement structure. The sensors embedded in the pavement collect environmental information which is read through RF transmission using an RF reader that is either manually operated or mounted on a moving vehicle. By directly equipping the vehicle with low-cost RF transponders, the roads can be frequently monitored to detect changes in structural integrity which helps for accurate scheduling of preservation measures.

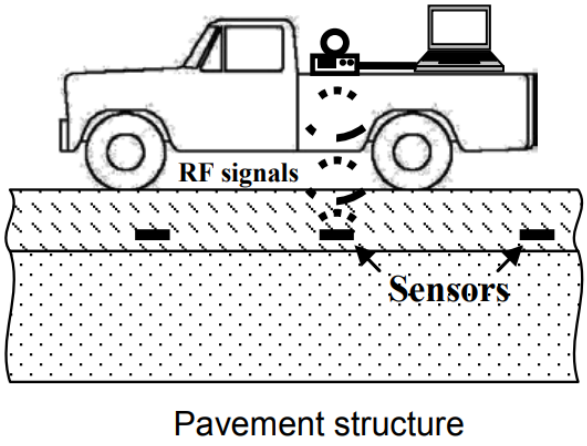

Figure 1. Illustration of the system in case 1 [5].

The second approach, discussed in [6], presents a wireless sensor network that can also collect and deliver pavement data, as is shown in Figure 2. The system consists of wireless sensor nodes that are embedded in the pavement (shown in red circles) and an access point installed on the roadside. Similarly, the sensor nodes are self-powered and are able to collect environmental data from time to time. The access point on the roadside consists of RF receivers

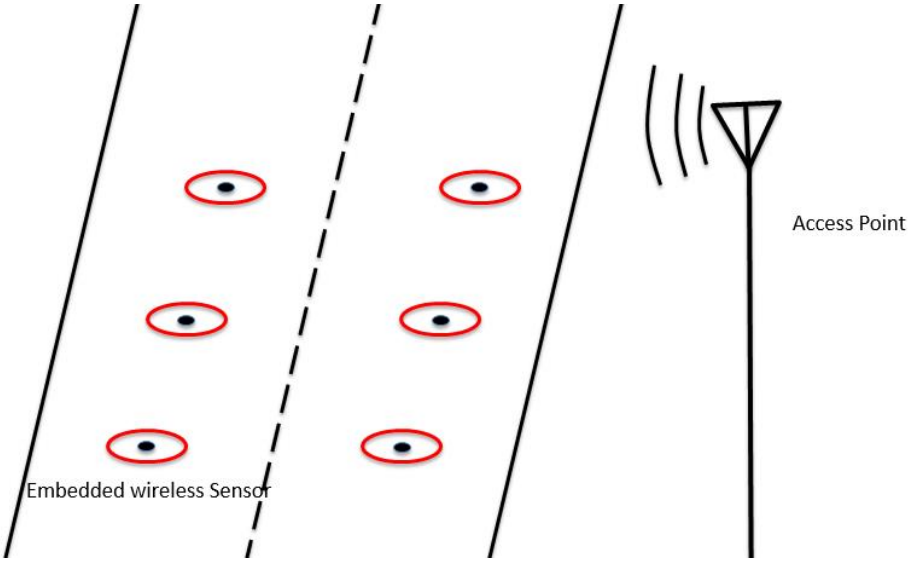

Figure 2. Illustration of the system in case 2 adapted from [6].

which gather the information sent by the RF transceivers that are attached to the sensors. The data are synchronized and can be viewed on terminals which are in the same LAN with the access point.

Comparisons are made in order to decide which system to use. The advantage of the system in the first case is that at the operating frequency of around 13 MHz, the attenuation of the signals in transmission will be relatively small. Furthermore, since RFID readers and transponders are relatively cheap, the system can be built cost-effectively. However, this system requires cars to drive over the sensors to collect data, making the system less convenient and more costly to operate. In contrast, by using wireless sensors, the system in the second case can collect and deliver data without manual operation. Moreover, the system has a bigger bandwidth of 75 MHz compared to the bandwidth of 2 MHz for the RFID reader. Unfortunately, signals experience more attenuation in the second case because the system operates at a much higher frequency of 2.4 GHz.

Considering the ease of data collection and overall cost, the second system outranks the first. Although off-the-shelf antennas can be used in the system design, drawbacks have been found regarding the increase of power consumption and decrease of system lifetime. Therefore, to maximize the performance of the embedded antenna, I chose to design one for the second system.

2.2 Previous Work

2.2.1 Standard Patch Antenna Used under Pavement

Much work involving smart pavement monitoring systems has been done. One of the most typical examples of using wireless sensor nodes for delivering information is included in [6], where the sensors, wireless transceiver, and batteries are packaged into a small box that is placed under the pavement. To save more room for other components in the box, Bajwa [6] used a commercial patch antenna (CC2420, Texas Instruments) in his embedded system, which results in a potential future problem. Since wireless sensors are intended to be embedded in

the pavement for long-term use (usually for more than 10 years), power consumption becomes a key factor in determining the lifetime of the system. Because CC2420 operates at 2.4 GHz to transmit signals, a significant loss of signal strength from transmission through pavement will be introduced. A simple calculation follows to explain why antennas which operate at relatively high frequency are ill-suited for use used under pavement.

By the Friis transmission equation, power received by the receiving antenna is

$$P_r = \frac{P_t G_t G_r \lambda^2}{(4\pi R)^2} \cdot loss \quad (2.1)$$

where P_t is the transmitted power; G_t and G_r are the gains of the transmitting and receiving antenna, respectively; λ is the wavelength; and R is the path length. As is known,

$$loss \propto (e^{-\alpha d})^2 \quad (2.2)$$

where α is the attenuation factor, and d is the thickness of the pavement. In the case of imperfect dielectric material, such as pavement,

$$\alpha = \frac{\sigma}{2}\sqrt{\frac{\mu}{\epsilon}} \quad (2.3)$$

and loss tangent is related to the conductivity by

$$tan\delta = \frac{\sigma}{\epsilon\omega} \quad (2.4)$$

So the attenuation factor can be expressed as

$$\alpha = \frac{\pi\sqrt{\epsilon_r}}{\lambda} tan\delta \quad (2.5)$$

The permittivity, loss tangent and thickness of the pavement are 6, 0.02 and 7.62 cm (3 inches), respectively [7]; and G_t, G_r, R are 1 dB, 1 dB, and 4 m, respectively. Therefore, the ratio of the received power over the transmitted power is

$$\frac{P_r}{P_t} = \frac{G_t G_r c^2}{(4\pi R)^2} \cdot \frac{1}{f^2} e^{\frac{-2\pi d\sqrt{\epsilon_r} tan\delta}{c} \cdot f} \quad (2.6)$$

and attenuation is calculated by

$$Attenuation = -10log_{10}\left(\frac{P_r}{P_t}\right) \quad (2.7)$$

Figure 3 shows the attenuation of signals when frequency varies from 100 MHz to 10 GHz. It can be observed that the attenuation has a direct relationship with frequency and starts to increase faster when frequency is over 1 GHz. Therefore, in order to reduce power loss in the pavement, antennas of relatively low frequency should be used.

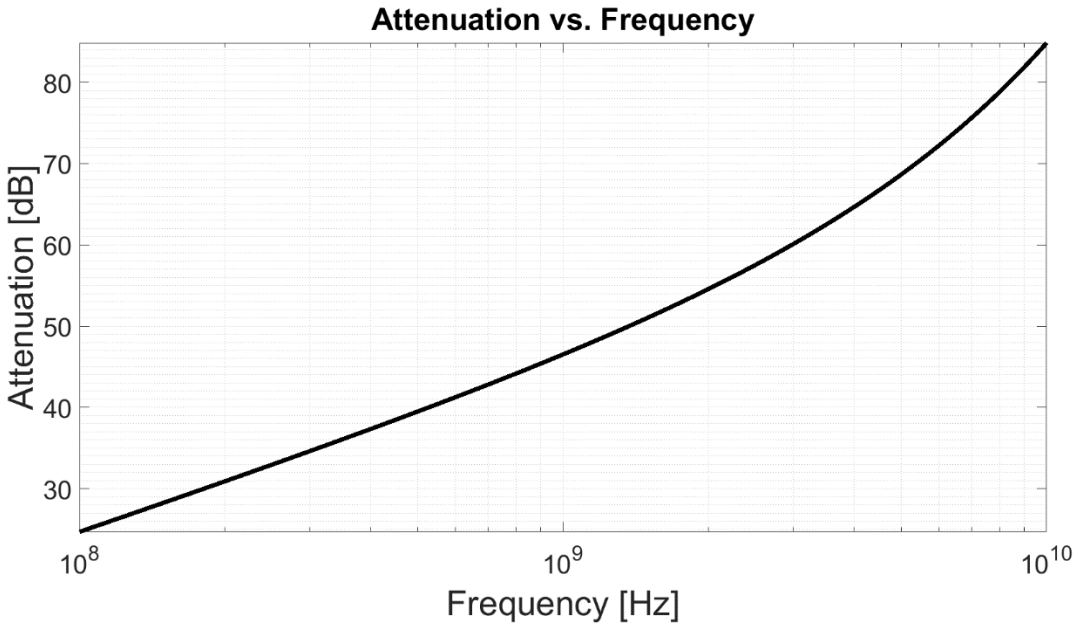

Figure 3. Attenuation vs. frequency.

2.2.2 Standard Loop Antenna Used under Pavement

Another research example of an embedded antenna is that of Akkari et al. [8], who experimented by embedding two loop antennas under the pavement to test their communication range. The two loop antennas are placed vertically and are at the same depth, as is shown in the Figure 4. There are two communication paths that signals can take: one is through the air, and the other one is through the pavement. Generally, it is difficult for signals

of a transmitting antenna to travel to a receiving antenna through a curvature path without rectification of other devices. As a consequence, only a small portion of signals can be sent to their destination. Unfortunately, signals travelling through pavement also experience significant power loss. As is indicated in (2.2), given a fixed attenuation coefficient, the loss generated in lossy material is proportional to d^2. Obviously, the farther a signal travels through pavement, the greater its attenuation.

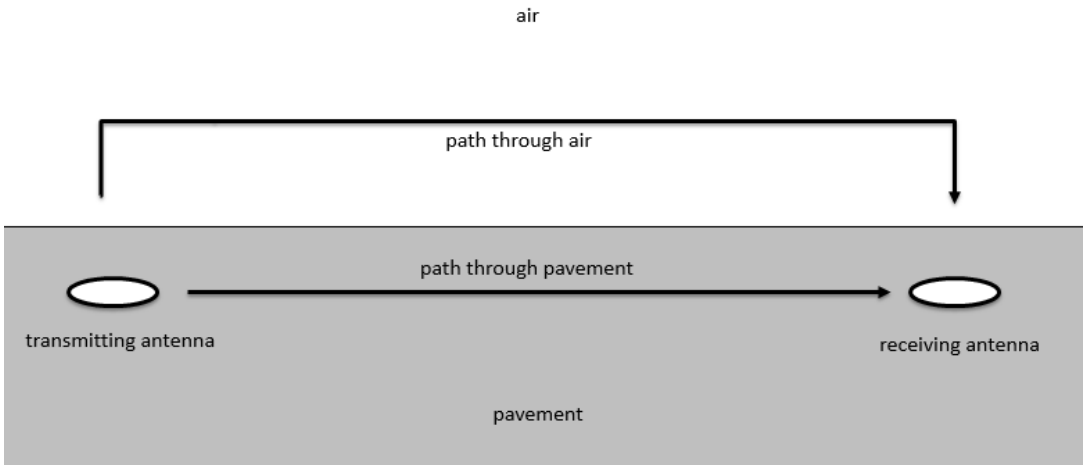

Figure 4. Illustration of a two-communication path model of embedded antenna adapted from [8].

The result of Akkari et al.'s test for the range is about 6 m. The poor communication range comes from two aspects. First, since they used an off-the-shelf circular shaped antenna, the signals travel omnidirectionally. Thus, the majority of the signal transmitted to the receiving antenna goes through the pavement rather than through the air, which gives rise to the heavy attenuation of the signal. Second, the impedances of the antennas used in the experiment are not well matched, which results in unsatisfactory radiation efficiency. Both of these issues can significantly increase the power consumption of the antenna. Furthermore, loop antennas are not the best choice for packaging because they usually take more space than other low-profile antennas.

2.2.3 Low-profile Antennas for IoT Applications

Recent years have witnessed the proliferation of antennas designed for IoT applications. Although serving different research goals, most of these antennas are based on the microstrip patch antenna (MSA) because of its innate merits such as compact size, light weight, and great performance in communications. Therefore, MSAs are widely used in IoT areas, especially in the field of wearable devices.

When designing an antenna, it is necessary to consider any changes to signals in their transmission paths. Similar to the embedded antenna, whose signal is affected by the pavement above it, an antenna used in a wearable device also has the problem of its signals being disturbed by lossy material like skin and clothes. Lee and Choi [9] researched a polarization reconfigurable patch antenna for wearable IoT applications. The antenna suggested has better power gain and bandwidth than regular patch antennas, and the capability of producing three different polarization modes. Although detailed description concerning functionality and design of the antenna is given in [9], information about the general design of IoT antennas can hardly be found. Likewise, many research papers focus on a specific design for a certain application and neglect the common design procedure that most IoT antennas share.

2.2.4 Summary for Background

With the increasing need to monitor the health and wellness of aged infrastructure, smart pavement monitoring systems have been proposed and researched. Despite the fact that much research work has been done to design and develop the monitoring systems, nearly none of the work focuses on improving the performance of antennas. Since the embedded monitoring system placed under the pavement is intended for long-term use, it is critical to redesign the antenna, which is one of the major power-consumption devices. Drawbacks and flaws are found in relevant previous work, which comprise three main aspects: inappropriate frequency, path loss, and impedance mismatch. These can be viewed as the key factors when designing new antennas for the system.

Given the fast development of IoT antennas, it is reasonable to expect more engineers to enter this area. Unfortunately, it is found that most of the papers regarding embedded IoT antennas lack a general procedure for the design process, which detracts from the popularization of IoT antennas.

Chapter 3

Theory

3.1 Overview

In order to illustrate how to develop an embedded antenna for IoT applications, the detailed design procedure will be covered in this chapter. Using an example of an embedded antenna applied in a smart pavement monitoring system, we will discuss the following steps of the design process:

- Antenna selection
- Frequency selection
- Model construction
- Ground plane improvement
- Simulation
- Design verification

The steps above can serve as a basic reference procedure for beginners who are not familiar with embedded IoT antenna. Based on practical requirements, designers can by all means add more features to realize the best performance in actual situations.

After the last steps of simulation and verification, the proposed antenna will be fabricated and measured, which will be discussed in Chapter 4.

3.2 Design Procedure

3.2.1 Antenna Selection

The antenna is one of the oldest applications in the field of electromagnetics and has been researched for more than a century. Over time, antennas have become more diverse in terms

of their shapes and functionalities. Nowadays, there are various types of antennas that are available to use, such as dipoles, patch antennas, loop antennas and horn antennas. Despite the fact that many antennas have similar performance, the selection of an antenna should consider the practical situation.

In our case of designing an embedded antenna for a smart pavement monitoring system, the size of the proposed antenna cannot be too big, since the antenna needs to be packaged into a small box. For this reason, a low-profile antenna becomes our preferred choice. As is mentioned, the MSA is one of the widely used low-profile antennas in IoT technology because of its shape and functionality, which allow it to be mounted on small devices conveniently. Moreover, considering the ease of design and reliability of implementation, MSA is a good model to illustrate the design procedure. As a result, it is selected as the design prototype in this work.

3.2.2 Frequency Selection

Besides the antenna model, frequency is another important factor to be considered. Even among antennas of the same type, the operating frequency can have a big effect on both size and path loss. In contrast to most of the commercial antennas, such as D-Link DWL-R60AT, XBEE-Pro S1, and V-link Wireless Voltage Node, which operate at 2.4 GHz, the proposed MSA is to be designed to operate on a lower frequency band in order to reduce the signal attenuation along the transmission path. For legal usage, the operating frequency is chosen to be at 915 MHz, which is the center frequency of one of the unlicensed ISM bands for mobile applications. The reason for not going down to 433 MHz is that the dimensions of the antenna would nearly double, as is indicated in the equation for calculating the length of a half-wave rectangular MSA [10]:

$$L \approx 0.49\frac{\lambda}{\sqrt{\epsilon_r}} = 0.49\frac{c}{\sqrt{\epsilon_r} f} \quad (3.1)$$

To decrease the dimensions of the proposed MSA given the frequency, a microstrip material (Duroid® 6010LM substrate) with high relative permittivity of 10.2 is chosen. Therefore, by

rough calculation, the length of the patch is about 5 cm. With the consideration of the ground plane, the overall size of 10 cm × 10 cm is preferred in this research.

3.2.3 Model Construction

The MSA has been one of the most widely used antennas since it came out during the 1950s. Much research about MSA has been completed to perfect its theory and improve its performance. Nowadays, it is not difficult to study how to design a regular MSA for given specifications provided that there are no obstacles in the signal transmission path. Nonetheless, when developing IoT antennas, designers should be aware of the lossy material that is near the antenna. For instance, when there is pavement above the antenna, the resonating frequency and radiation pattern are not what they would be otherwise.

In order to maintain the radiation properties of the MSA, propagation through the pavement has to be taken into consideration. A powerful approach is adopted in this research to solve the pavement question. We aim to model the antenna together with the pavement to calculate the effective permittivity of the substrate for the MSA. Once the effective permittivity is calculated, we can use it to determine the dimensions of the MSA and then to adjust the parameters of the antenna accordingly. But before we discuss the construction of pavement-antenna model, basic theory of MSA should be studied for further understanding.

The cavity model has been used as one of the most popular ways to analyze the rectangular MSA. It represents the rectangular MSA as an array of two parallel slots, which are the sources for radiation in the far field [10].

Since the dimensions of the patch are finite, fringing fields occur at the edges, causing the two identical slots to appear, which is illustrated in Figure 5. Because of that, the electrical length of the patch is greater than its physical length. To keep the frequency constant, the length is modified as [10]

$$L = \frac{c}{2\sqrt{\epsilon_{eff}} f_r} - 2\Delta L \qquad (3.2)$$

where ϵ_{eff} is the effective dielectric permittivity and ΔL is the length of the slot.

Figure 5. Top view of the cavity model adapted from [10].

By studying and summarizing experimental data, the fringing length is modeled as [10]

$$\Delta L = 0.412 \frac{\left(\epsilon_{eff} + 0.3\right)\left(\frac{W}{t} + 0.264\right)}{\left(\epsilon_{eff} - 0.258\right)\left(\frac{W}{t} + 0.8\right)} \qquad (3.3)$$

where W is the width of the patch and t is the thickness of the substrate.

There are different ways to determine the width of the patch based on which optimizing value is focused on. For example, if the input impedance is set to a certain value, then the width can be found from [10]

$$\mathrm{Z}_A = 90 \frac{\epsilon_{eff}^2}{\epsilon_{eff} - 1} \left(\frac{L}{W}\right)^2 \Omega \qquad (3.4)$$

Or if bandwidth is the goal, the width can be calculated from [10]

$$BW = 3.77\frac{\epsilon_{eff} - 1}{\epsilon_{eff}^2}\frac{W}{L}\frac{t}{\lambda} \quad (3.5)$$

In this research, since an MSA of high efficiency is preferred, the width is determined by [10]

$$W = \frac{\lambda}{2}\left[\frac{\epsilon_{eff} + 1}{2}\right]^{-\frac{1}{2}} \quad (3.6)$$

With the knowledge of traditional MSA, we can proceed to the construction of the pavement-antenna model. Figure 6 shows the model of the embedded antenna structure where a layer of pavement with an air gap is placed above the MSA.

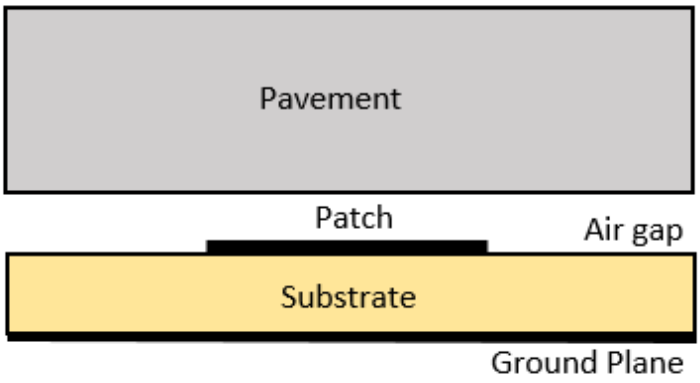

Figure 6. Cross section of the embedded antenna structure adapted from [12].

Again, the purpose of constructing this model is to determine the effective permittivity (ϵ_{eff}) of the substrate. Several researchers have explored developing an accurate closed equation to calculate ϵ_{eff} using the method of conformal mapping, which was first proposed by Wheeler [11]. Later, Bernhard and Tousignant [12] improved the accuracy of the method by using a more accurate physical model which is similar to the one shown in Figure 6.

Based on the method in [12], the effective permittivity is determined by a combination of the dimensions of the MSA, and permittivities and sizes of different layers, as is shown below [12]:

$$\epsilon_{eff} = \epsilon_{r1}q_1 + \epsilon_{r1}(1-q_1)^2 \times [\epsilon_{r2}^2 q_2 q_3 + \epsilon_{r2}\epsilon_{r3}(q_2 q_4 + (q_3+q_4)^2)] \times [\epsilon_{r2}^2 q_2 q_3 q_4 + \epsilon_{r1}(\epsilon_{r2}q_3 + \epsilon_{r3}q_4)(1-q_1-q_4)^2 + \epsilon_{r2}\epsilon_{r3}q_4(q_2 q_4 + (q_3+q_4)^2)]^{-1} \quad (3.7)$$

where $q_i, i = 1,2,3,4$ are the filling fractions determined by conformal mapping.

Provided with ϵ_{eff} and frequency, the length and width of the patch can then be back-solved from (3.2)-(3.6) and the design process in [12].

3.2.4 Ground Plane Issue

Using the method discussed in the previous section, we have finished the initial design of the embedded MSA. Unfortunately, from the simulation result of HFSS, this antenna is not able to provide enough gain in the far field. The reason for this is the discrepancy in the size of the ground between simulation and the model construction. The pavement-antenna model we used assumes that the size of the ground plane is infinity to simplify and enable the calculation for the closed equations. However, in reality the ground plane of the MSA cannot exceed the size of the box that contains the antenna, which is designed to be 10 cm × 10 cm. As a consequence, the initial design failed the requirement of specifications and needs to be modified.

It has been concluded that the limitation of designing rectangular MSA for packaging lies in the dimensions of the ground plane. Noghanian and Shafai [13] indicate that the radiation pattern of a rectangular MSA heavily depends on the size of its ground plane. This is because currents accumulated at the edge of a finite ground plane cause spurious radiation by the diffraction effect [14]. To see the influence of changing the ground plane size on the radiation pattern of a rectangular MSA, a series simulations have been done. The simulation was set up based on the model shown in Figure 6 with the list of parameters indicated in Table 1. The simulation result is shown in Table 2.

Table 1. Design parameters for the simulation set-up

Design parameters	Value	Electrical dimension
Pavement relative dielectric	6	
Pavement thickness	7.62 cm	
Air gap thickness	1.5 cm	0.70 λ
Substrate relative dielectric	10.2	0.14 λ
Resonating frequency	915 MHz	
Patch width	6.74 cm	0.62 λ
Patch length	4.96 cm	0.46 λ

Table 2. Gain vs. ground plane size

Ground plane size in wavelength	Gain [dB]
width * length	-0.84
(width + $\frac{1}{16}$ λ) * (length + $\frac{1}{16}$ λ)	-0.28
(width + $\frac{1}{8}$ λ) * (length + $\frac{1}{8}$ λ)	1.42
(width + $\frac{1}{4}$ λ) * (length + $\frac{1}{4}$ λ)	1.66
(width + $\frac{1}{2}$ λ) * (length + $\frac{1}{2}$ λ)	2.58
(width + $\frac{3}{4}$ λ) * (length + $\frac{3}{4}$ λ)	2.97

It can be observed from the result that the trade-off in design is between the dimensions of the ground plane and the gain, which are two significant parameters that engineers have to balance during the design of MSAs. In IoT antenna designs, it is important to make the device portable and functional at the same time. Therefore, the issue here becomes how to maintain the gain

of the antenna while keeping the ground plane within acceptable size, which requires other techniques to help solve this problem.

3.2.5 Ground Plane Improvement

It is known that one of the methods to diminish the diffraction effect at the edge of a finite ground plane is to reduce the surface current around its boundary. As is indicated in [15], applying serrations to the ground plane can help reduce this effect by forcing current to circulate at the edge of the ground plane [15]. Thus, the on-going current flowing to the serrations will be cancelled out by the trapped current. This technique allows less current to be reflected back from the edge of the ground plane. Therefore, the serrated ground plane becomes electrically bigger than its physical size.

To have an intuitive sense of how current behaves when encountering serrations at the edge of the ground plane, regular and serrated MSA models were built in HFSS to simulate the two different situations for the surface current.

The simulation result in Figure 7 shows the magnitude of surface current on the regular ground plane and the serrated one. The two MSAs have the same size and were simulated in the same environment shown in Figure 6. It can be seen that the edge current on the serrated ground plane is less than that on the regular ground plane, which indicates that serrations can be used as a means to reduce edge current.

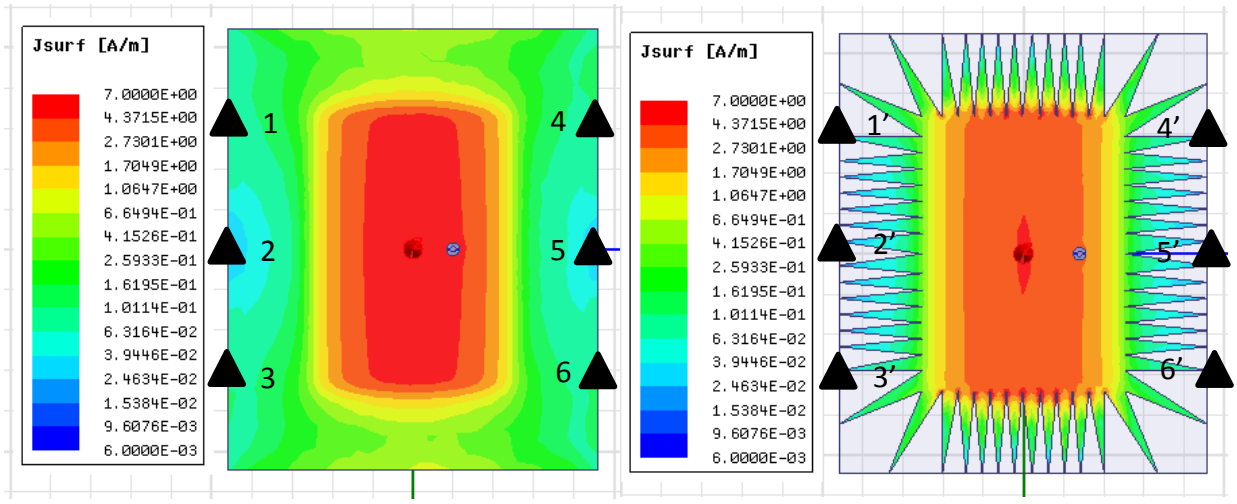

Marker Table	
Current [mA/m]	Current [mA/m]
1: 50.2	1’: 19.6
2: 23.1	2’: 8.47
3: 49.6	3’: 21.4
4: 51.1	4’: 18.5
5: 18.8	5’: 8.59
6: 52.3	6’: 20.6

Figure 7. Comparison of current distribution on regular ground plane (left) and serrated ground plane (right).

To explore the relationship between the dimensions of serrations and the gain, serrations of different sizes on the same ground plane of an MSA were tested. We selected the two most representative examples to explain.

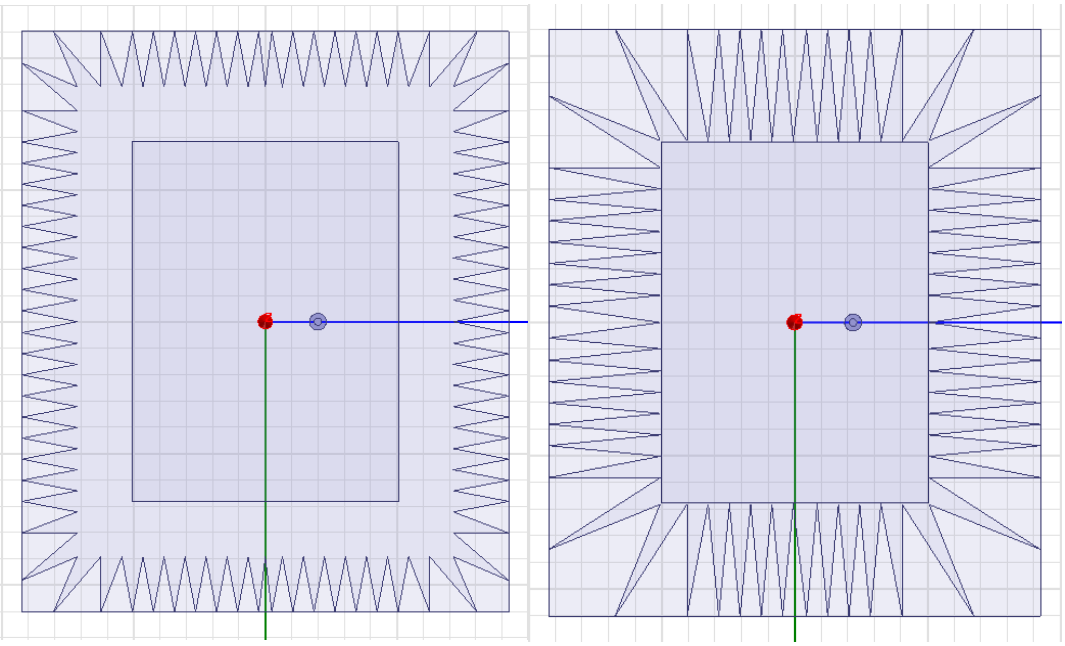

Figure 8. Moderately serrated MSA (left) and fully serrated MSA (right).

Figure 8 shows two common types of serrations applied onto the ground plane. As is seen, one of the ground planes is moderately serrated, and the other is fully serrated. The dimensions of the moderate serration are roughly half those of the full one. Applying the models to HFSS, the simulation result of the two is shown in Table 2. The design parameters for the simulations are the same as those shown in Table 1.

Table 3 shows the simulation result for gains of antennas when different serrations are applied to their ground planes. It can be seen that with the increase of the dimension of the serration, the gain of the MSA is gradually improved. One may notice that the sizes of the ground planes are not the same even if the serrations are applied to the same MSA. In order to achieve impedance match at the input port of the MSA, the dimension of the patch is slightly modified according to which kind of serration is used.

Table 3. Effect of different types of serrations on gain and ground plane size

	MSA w/o serrations	Moderately serrated MSA	Fully serrated MSA
Gain [dB]	1.42	2.17	2.50
Ground plane size [cm]	11.02 * 9.25	10.95 * 9.16	10.85 * 9.10
Electrical dimension	1.01 λ * 0.85 λ	1.0 λ * 0.84 λ	0.98 λ * 0.83 λ

It can be concluded from the simulation result that applying serrations to the ground plane can not only increase the gain of the antenna, but also slightly decrease the size of the ground plane. Hence, the technique of applying serrations is considered an effective method to boost the gain while maintaining the size of the ground plane.

3.2.6 Pavement Sensitivity Analysis

Now that most of the design procedure has been illustrated, we are able to design an embedded IoT antenna for the purpose of general usage. However, because part of the theory we discussed is based on an ideal case, antenna performance will be different from the design in reality. Among all the issues posed by practical situations, pavement inconsistency is the one that influences the radiation pattern of the antenna most. During the design procedure, the pavement is assumed to have constant thickness and unchanged permittivity, which simplifies the calculation and model construction. Yet in the actual construction of road, it is very hard to keep the pavement at the same thickness. Furthermore, when maintaining aged road, workers can hardly repair a broken area at the same thickness as other parts of the road. In addition, during rain or snow, the permittivity of the pavement is likely to change. As a consequence, it is necessary for engineers to know the radiation pattern of the designed antenna when the pavement parameters deviate from their original values.

To perform the sensitivity analysis, the proposed antenna was tested in HFSS for the following changes in pavement parameters: relative permittivity, loss tangent and thickness.

According to [16], the relative permittivity of asphalt varies with its condition. Table 4 shows the results of broadside gain of the antenna when the relative permittivity of asphalt pavement is swept from 4 to 7 to demonstrate the gradual change of pavement condition from dry to wet.

Table 4. Broadside gain vs. permittivity

Relative permittivity	Gain [dB]
4	3.06
5	3.09
6 (original)	3.47
7	3.30

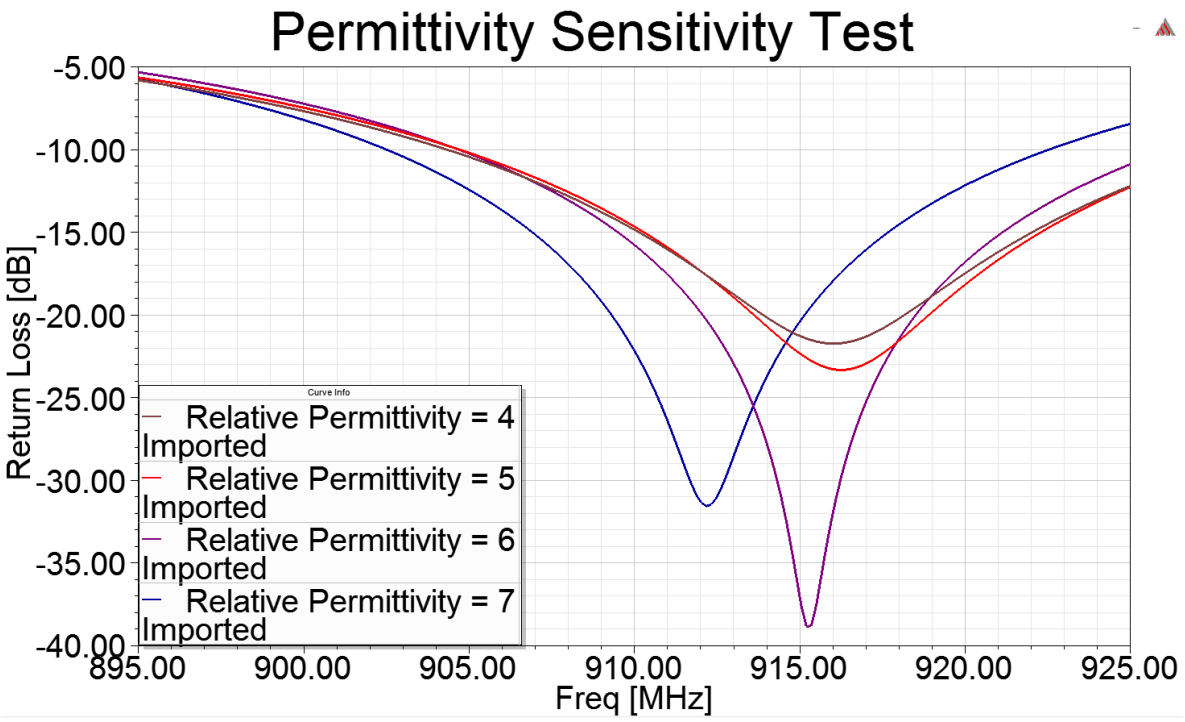

Figure 9. Return loss vs. permittivity.

It is observed that the antenna is able to sustain its broadside gain above 3 dB given predicted permittivities of asphalt pavement. The variation in gain results from impedance match, as is shown in Figure 9. Bernhard and Tousignant [12] indicate that increasing permittivity of the pavement can raise the effective permittivity of the antenna model. Therefore, by equation (3.1), the resonating frequency of the antenna decreases with the increase of its effective permittivity, which causes the difference in gain.

Table 5. Broadside gain vs. loss tangent

Loss tangent	Gain [dB]
0	5.47
0.04	4.78
0.08	4.09
0.12 (original)	3.47
0.16	2.89
0.2	2.28

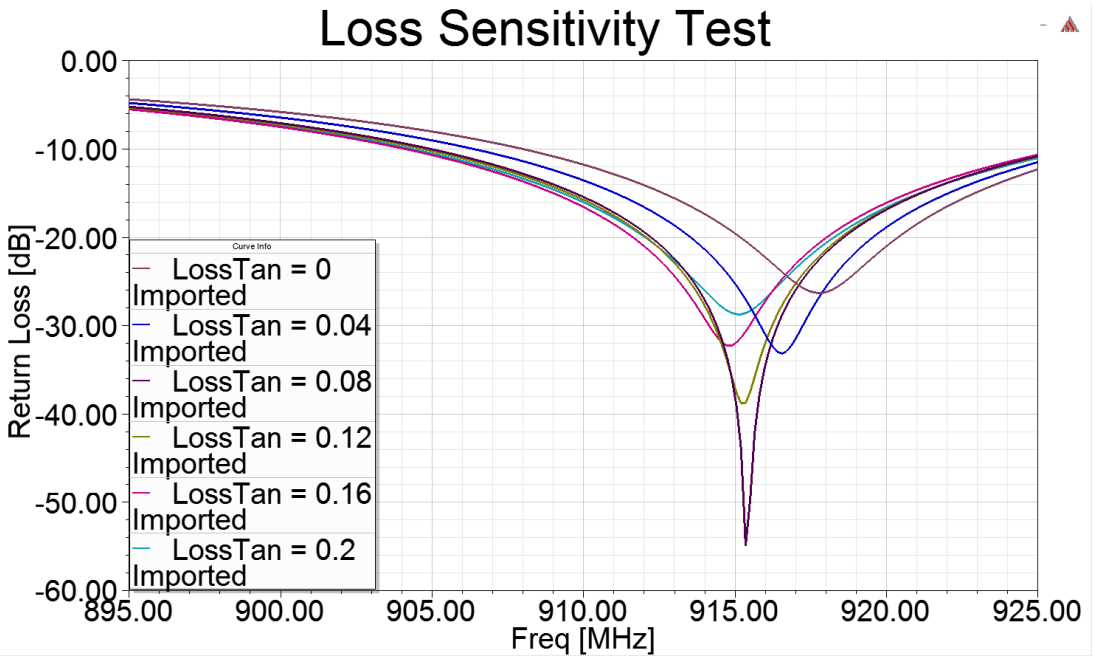

Figure 10. Return loss vs. loss tangent.

Loss tangent is another pavement parameter that is likely to be affected by weather. For example, when it rains the loss tangent of asphalt pavement will increase to 0.2 [17]. Table 5 and Figure 10 demonstrate the influence of change of loss tangent on radiation pattern and return loss of the antenna, respectively. It can be seen that the broadside gain of the antenna decreases with the increase of loss tangent of the pavement. Although the antenna is designed under the assumption that the loss tangent of the pavement is 0.12, it has the capability to maintain its performance when the loss tangent of the pavement changes within 0 to 0.2.

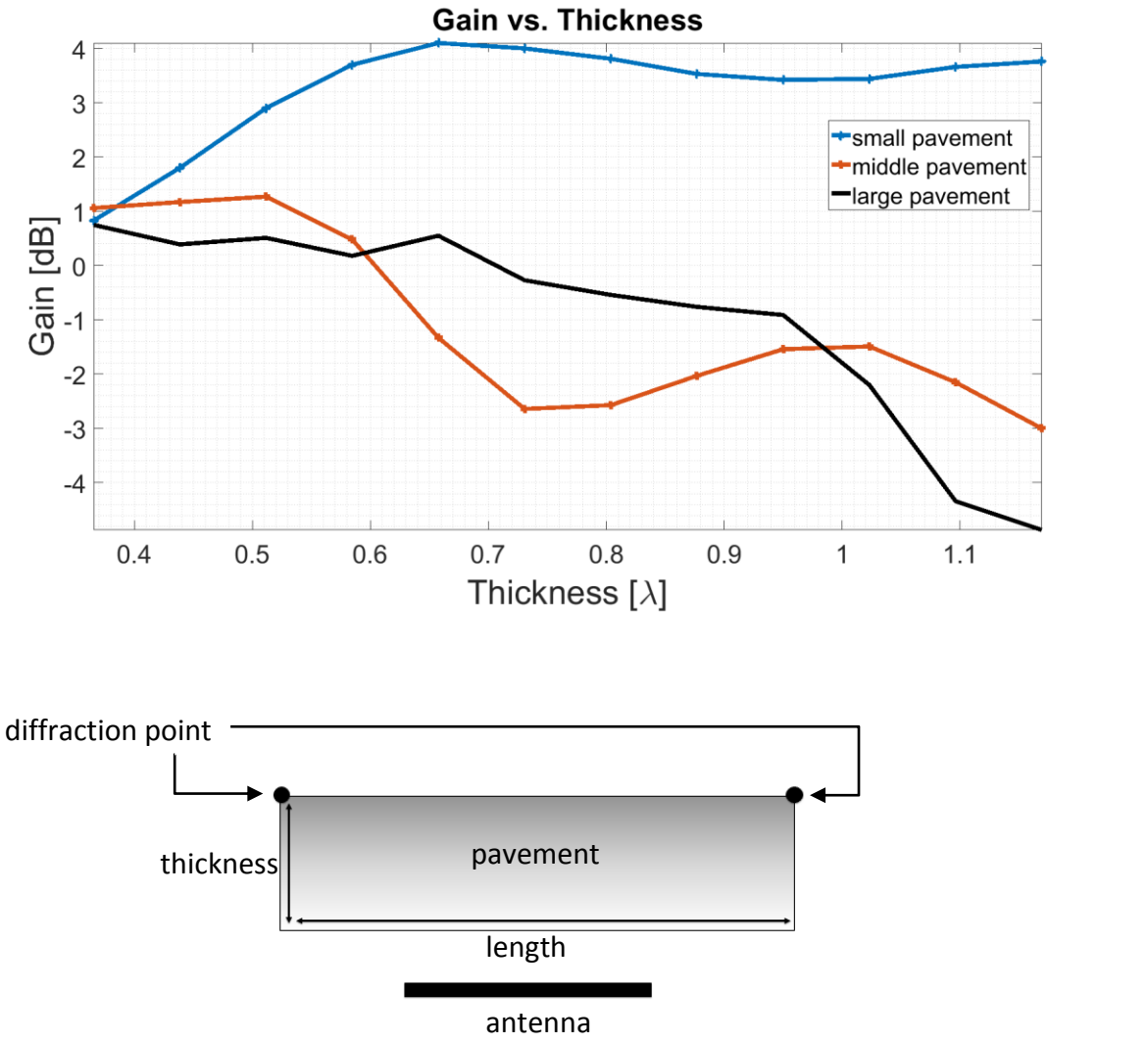

Figure 11. Gain vs. thickness with different sizes of pavement (top) and simple model for illustration (bottom).

Figure 11 shows the change in broadside gain of the proposed antenna with different pavements, the thickness of which varies from 5 to 16 cm (the unit of thickness has been converted to wavelength in Figure 11). One may find it unusual that with the small pavement (length = 30 cm/2.2 λ), the gain of the antenna has a direct relationship with the thickness of the pavement since the antenna gain is supposed to decrease when lossy material is placed above it. The reason for this unexpected result is likely from the lensing effect and the diffraction effect of the finite pavement. The lensing effect occurs when waves reflect at the side surfaces of the pavement, which helps EM waves focus at broadside to increase the gain of the MSA, while the diffraction effect occurs at edge corners of the pavement and can increase the gain. If the dimension of the pavement is set to be big enough in simulation, the lensing effect disappears and the relationship between the broadside gain and pavement thickness becomes inverse, which can be observed with the case of large pavement (length = 78 cm/5.7 λ).

Because of the cylindrical pavement samples used in the antenna model, the radiation pattern shown in Figure 11 is not able to reflect the actual performance of the proposed MSA with infinite pavement. It can also be seen that the performance of the antenna is below our expectations when large pavement is used. Therefore, the design model has to be improved based on real situations, which is considered as one of the future tasks. The fluctuation of the gain with increase of the thickness is due to impedance mismatch, which also affects the radiation pattern in permittivity test.

The pavement sensitivity analysis provides information about performances of the proposed antenna when the pavement parameters are changed, and allows us to prepare for environmental influence on the antenna under various situations. Despite that the sensitivity analysis only studies the effects of three parameters, those are the factors that can have major influences on the performance of the proposed antenna. By all means, designers can run sensitivity analysis based on different parameters that can significantly affect their IoT antennas.

Chapter 4

Measurement

4.1 Antenna Fabrication

Now that we have a complete design of the embedded IoT antenna, the next step is to fabricate the proposed antenna for measurement.

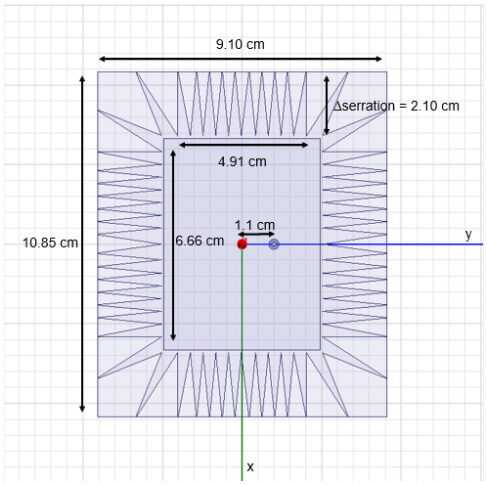

(a)

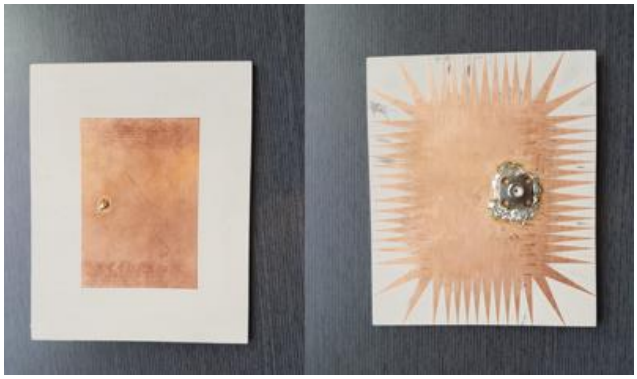

(b)

Figure 12. (a) Top view of the proposed MSA; (b) Top (left) and bottom (right) of the fabricated MSA.

Figure 12(a) shows the top view of the proposed MSA, whose dimensions and serration size are obtained using the techniques discussed in Chapter 3. In order to achieve impedance match at the input port, the feed needs to be placed appropriately. Although there are equations for calculating the feed location in theory, it is much more efficient to determine where to add the feed experimentally. Parametric optimization was performed in HFSS to find the location that gives the lowest return loss at input port. Figure 13 shows the return loss of parametric optimization where the feeding point is tested at different locations along the y axis. Since the patch is symmetric around the x axis, only the right half plane is simulated.

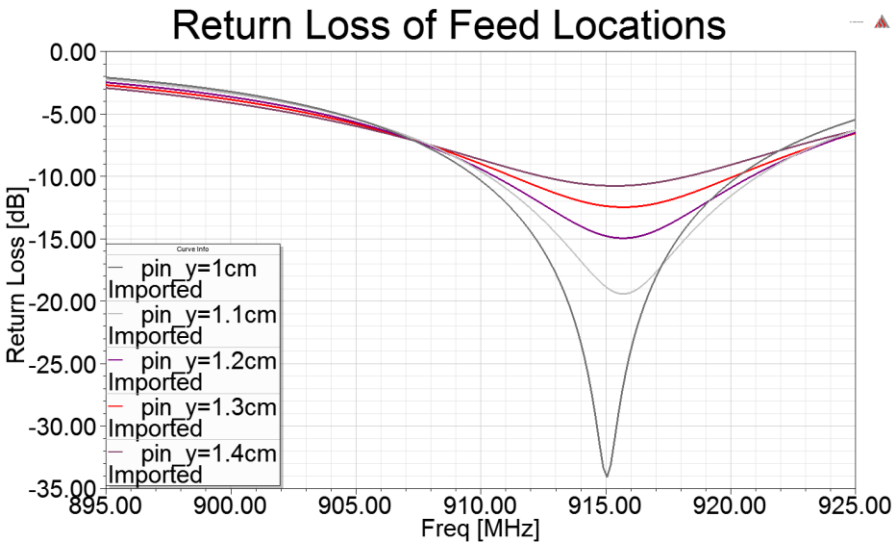

Figure 13. Parametric sweep of feed point location and resulting return loss.

From the result, the feed should be placed at 1.1 cm away from the origin to obtain the smallest return loss.

Figure 12(b) shows the fabricated MSA done by a milling machine. The patch is shown on the left, and the serrated ground plane is shown on the right. The SMA connector was soldered at the feed on the ground plane. During soldering, it is suggested to seal all the edges of the base of the SMA connector to prevent loss of signals.

4.2 Pattern Measurement

Figure 14 demonstrates the basic setup for the measurement of the proposed embedded IoT antenna, where two cylindrical pavements made of asphalt are placed above the MSA to mimic the real situation of pavement. The top rectangle shows the dimensions of the patch, which correspond to the top layer in the antenna model.

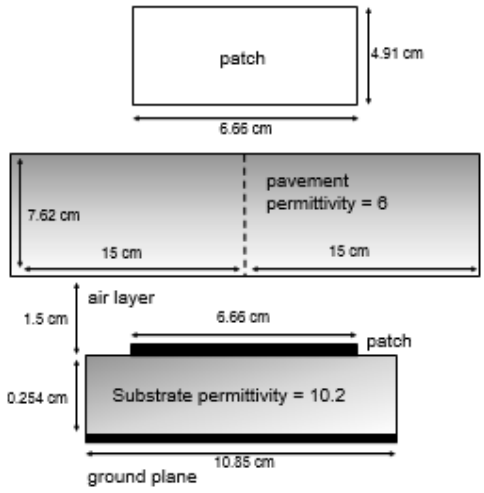

Figure 14. Measurement setup.

To avoid interference from outside signals as well as to simulate far field condition, an anechoic chamber was used. The physical setup for the measurement is displayed in Figure 15.

Figure 15. Measurement setup in the chamber.

The method of link budget is adopted to calculate the gain of the antenna under test.

Similar to performing regular RF measurement, the first step is to calibrate the system to remove the impact of noise and loss from cables and measurement equipment. To implement calibration, two standard gain horns (SGHs) were placed at the transmitter and receiver end. In Figure 15, the receiver end is where the SGH is placed while the transmitter end is where the pavement-antenna model is set up. After acquiring the gain for the SGH ($\mathrm{S21_{sgh}}$), we replaced the SGH at the transmitter end with the pavement-antenna model to obtain its relative gain with respect to the SGH ($\mathrm{S21_{aut}}$). Since the absolute gain of the SGH is known, we can thereby calculate the absolute gain of the embedded antenna by using the equation

$$Gain_{aut} = S21_{aut} - S21_{sgh} + Gain_{sgh}$$

where all of the variables are in dB.

4.3 Results

By now, we have successfully finished both the simulation and measurement for our proposed embedded antenna. In order to verify our design and to observe the discrepancy in the design, data of the radiation pattern and return loss from experiment and simulation are plotted together. Figure 16 shows the radiation patterns and Smith chart for the experiment and simulation. The simulation environment was built based on Figure 14. In order to resonate at 915 MHz, the dimensions of the patch for the MSA without serration are set to 6.78 × 4.98 cm, slightly different from those of the serrated MSA.

It can be seen that the measured gain has a good match with the simulated one in the case where serrations are applied to the ground plane, which verifies the correctness of the design procedure. As expected, the maximum gain increased by 1.9 dB with serrations added to the ground plane.

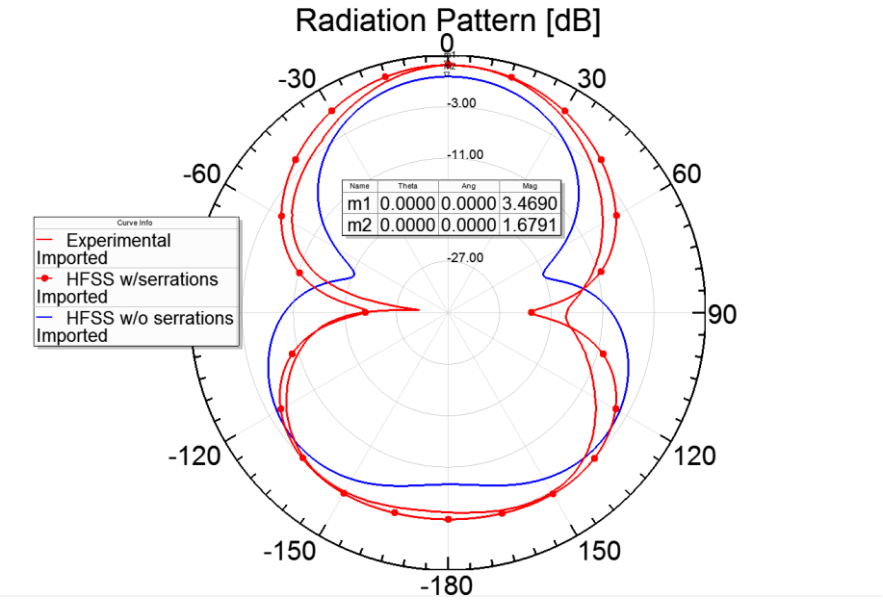

(a)

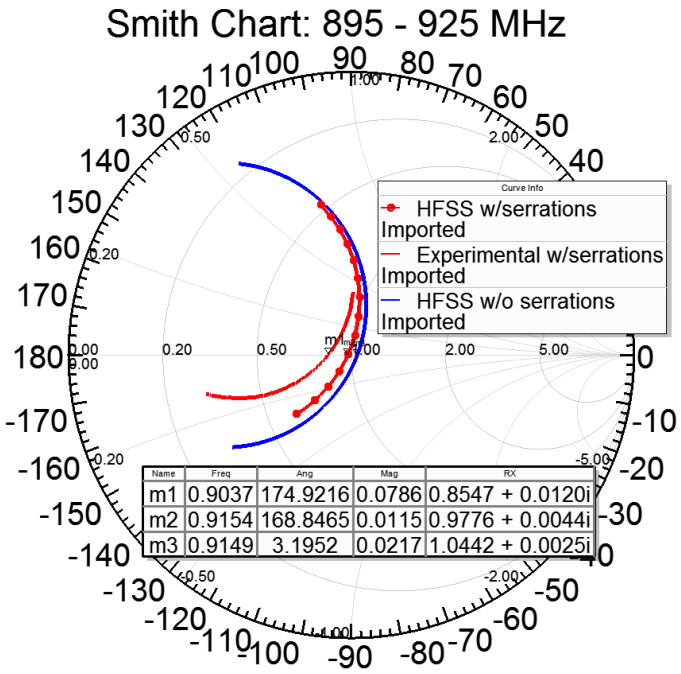

(b)

Figure 16. Radiation pattern and Smith chart from experiment and simulation. (a) Comparison of radiation patterns in E-plane (yz plane). (b) Comparison of Smith chart. Continued on next page.

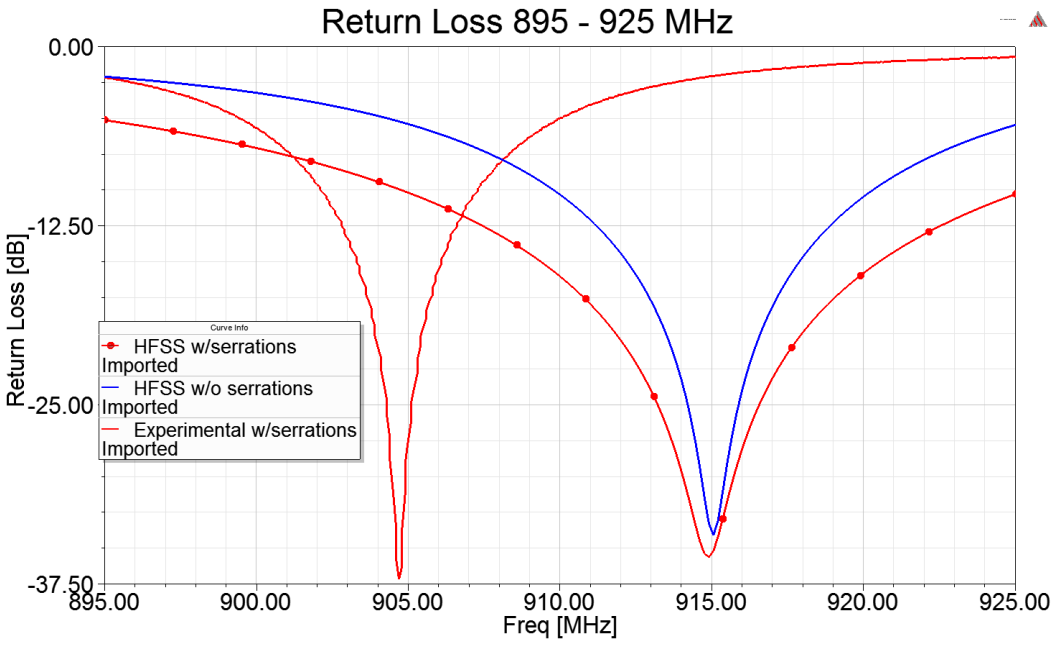

(c)

Figure 16 (continued). Radiation pattern and Smith Chart from experiment and simulation. (c) Comparison of return loss.

One may notice from the Smith chart of the experimental data that the fabricated MSA resonates around 904 MHz instead of 915 MHz as designed. The discrepancy comes from variations in the composition of the pavement samples and changes in pavement parameters, as is indicated in Section 3.2.6.

Chapter 5

Conclusion and Future Work

5.1 Conclusion

This thesis is an attempt to provide a general design procedure for IoT embedded antennas. With the increasing popularity of IoT devices, more and more engineers will enter this field. This work can serve as a general guideline for beginners to learn how to design an MSA for IoT applications.

To address the design procedure, a special case of smart pavement monitoring system has been studied and researched. The background information about the monitoring system is covered in Chapter 2, where previous work related to embedded antennas and IoT devices is discussed. By summarizing the common mistakes reflected in the earlier papers, we were able to find the places that can be modified and improved to make our antenna perform better.

Chapter 3 details the design procedure using an example of smart pavement monitoring system. It breaks the design process into six steps: frequency selection, antenna selection, model construction, ground plane improvement, simulation, and design verification. To start with, frequency and antenna model should be determined. Since MSA is one of the most widely used antennas in the IoT industry, it is chosen as the prototype for the design. After realizing that adding pavement above the antenna will change its radiation pattern, we constructed a model including the antenna and the pavement in order to accurately calculate the corresponding parameters for the antenna. It has been found in the simulation that the gain of an MSA with finite ground plane is reduced compared to that of an MSA with infinite ground plane. By applying serrations to the finite ground plane, we managed to achieve better gain. In the consideration of discrepancy in design resulting from deviation of pavement parameters in reality, sensitivity analysis has been performed to obtain relevant information so that proper modifications can be made to reduce negative impacts.

In Chapter 4, the fabricated IoT antenna has been shown together with the approach to determine the feed location to achieve impedance match. In addition, measurement steps are discussed to demonstrate how to measure gain of general antennas. Lastly, results from simulation and measurement have been compared and discussed. Overall, this work managed to provide the design procedure for a general IoT antenna with improvement.

5.2 Future Work

Regarding the model construction of the embedded antenna, there are several places that need to be modified and improved. First, this work only considers the case of pavement on top of the antenna; in order to characterize a more realistic environment, both top and bottom pavement should be considered in the design. Second, based on the simulation result in pavement sensitivity analysis (Section 3.2.6), the proposed MSA is not able to provide satisfactory gain when infinite pavement is placed above it. Therefore, the antenna has to be redesigned to pass the sensitivity test for practical usage.

As for the improvement in measurement, two cylindrical asphalt pavements need to be replaced with a large cubic asphalt sample to mimic the real situation. Moreover, to verify the results in sensitivity analysis, samples with different permittivity, loss tangent, and thickness should be tested for the antenna to prove its functionality under various conditions.

Generally, this work can be extended to other specialized antenna designs. Since most IoT antenna designs follow the general procedure discussed in Chapter 3, researchers and engineers can proceed similarly for more complicated antennas based on their own needs.

References

[1] S. Yang, K. Shen, H. Ceylan, “Integration of a prototype wireless communication system with micro-electromechanical temperature and humidity sensor for concrete pavement health monitoring,” *Cogent Engineering*, vol. 2, no. 1, 1014278, 2015.

[2] N. Barroca, L. M. Borges, F. J. Velez, F. Monteiro, M. Górski, J. Castro-Gomes, “Wireless sensor networks for temperature and humidity monitoring within concrete structures,” *Construction and Building Materials*, vol. 40, pp. 1156–1166, 2013.

[3] K. J. Loh, A. T. Zimmerman, J. P. Lynch, “Wireless monitoring techniques for structural health monitoring,” in *Proceedings of the International Symposium of Applied Electromagnetics & Mechanics*. Lansing, MI, 2007.

[4] 2014 Report Card for Illinois’ Infrastructure, webpage. Available at: http://www.isasce.org/wp-content/uploads/2014/04/2014-Illinois-Roads-Final-Report.pdf

[5] Federal Highway Administration, “Smart pavement monitoring system,” Technical Report FHWA-HRT-12-072, US Department of Transportation, 2013.

[6] R. Bajwa, “Wireless Weigh-In-Motion: Using road vibrations to estimate truck weights,” Technical Report, EECS Department, University of California, Berkeley, 2013.

[7] E. Jaselskis, J. Grigas, and A. Brilingas, “Dielectric properties of asphalt pavement,” *Journal of Materials in Civil Engineering*, vol. 15, no. 5, 2003.

[8] R. Akkari, J. Pei, T. Ibrahim, M. Zaman, P. Tang et al., “Initial design and validation of packaging directional antennas for structural health and road condition monitoring,” in *Proceedings of SPIE – The international Society for Optical Engineering*, 2011.

[9] H. Lee, J. Choi, “A polarization reconfigurable textile patch antenna for wearable IoT applications,” presented at International Symposium on Antennas and Propagation, Phuket, Thailand, 2017.

[10] W. Stutzman and G. Thiele, *Antenna Theory and Design.* NJ: John Wiley & Sons, 2012.

[11] H. A. Wheeler, "Transmission line properties of parallel wide strips by a conformal mapping approximation," *IEEE Trans. Microwave Theory Tech*., vol. MTT-12, no. 3, pp. 280, 1964.

[12] J. Bernhard and C. Tousignant "Resonant frequencies of rectangular microstrip antennas with flush and spaced dielectric superstrates," *IEEE Transactions on Antennas and Propagation*, vol. 47, no. 2, pp. 303-307, 1999.

[13] S. Noghanian and L. Shafai, "Control of microstrip antenna radiation characteristics by ground plane size and shape," *IEEE Antenna and Wireless Propagation Letters*, vol. 145, pp. 207-212, 1998.

[14] S. Manci, L. Borselli, and A. Cucurachi, "Diffraction from a truncated grounded dielectric slab: A comparative full wave/physical optics analysis," *IEEE Transactions on Antennas and Propagation*, vol. 48, pp. 48-57, 2000.

[15] G. Cung, G. Huff and J. Bernhard, "Ground plane edge serrations for improved performance of microstrip active reflectarray elements," *IEEE Antenna and Wireless Propagation Letters*, vol. 2, pp. 334-336, 2003.

[16] L. Liu, T. Guo, "Dielectric property of asphalt pavement specimens in dry, water-saturated, and frozen conditions," in *Proc. SPIE 4758, Ninth International Conference on Ground Penetrating Radar*, 2002.

[17] GPR Velocity Table and Analysis, webpage. Available at: http://gprrental.com/gpr-velocity-table-analysis/